

Schottky barrier height of epitaxial lattice-matched $\text{TiN}/\text{Al}_{0.72}\text{Sc}_{0.28}\text{N}$ metal/semiconductor superlattice interfaces for thermionic energy conversion

Cite as: Appl. Phys. Lett. **115**, 251901 (2019); <https://doi.org/10.1063/1.5126630>

Submitted: 05 September 2019 . Accepted: 03 December 2019 . Published Online: 18 December 2019

Sanjay Nayak , Shashidhara Acharya, Madhusmita Baral, Magnus Garbrecht , Tapas Ganguli, S. M. Shivaprasad , and Bivas Saha 



View Online



Export Citation



CrossMark

Lock-in Amplifiers
up to 600 MHz



Zurich
Instruments



Schottky barrier height of epitaxial lattice-matched TiN/Al_{0.72}Sc_{0.28}N metal/semiconductor superlattice interfaces for thermionic energy conversion

Cite as: Appl. Phys. Lett. **115**, 251901 (2019); doi: 10.1063/1.5126630

Submitted: 5 September 2019 · Accepted: 3 December 2019 ·

Published Online: 18 December 2019



View Online



Export Citation



CrossMark

Sanjay Nayak,^{1,2}  Shashidhara Acharya,² Madhusmita Baral,^{3,4} Magnus Garbrecht,⁵  Tapas Ganguli,^{3,4} S. M. Shivaprasad,^{1,2,6}  and Bivas Saha^{1,2,6,a)} 

AFFILIATIONS

¹Chemistry and Physics of Materials Unit, Jawaharlal Nehru Centre for Advanced Scientific Research, Bangalore 560064, India

²International Centre for Materials Science, Jawaharlal Nehru Centre for Advanced Scientific Research, Bangalore 560064, India

³Raja Ramanna Centre for Advanced Technology, Indore 452013, India

⁴Homi Bhabha National Institute, Training school complex, Anushakti Nagar, Mumbai 400094, India

⁵Australian Centre for Microscopy and Microanalysis, The University of Sydney, Camperdown, NSW 2006, Australia

⁶School of Advanced Materials (SAMat), Jawaharlal Nehru Centre for Advanced Scientific Research, Bangalore 560064, India

^{a)} Author to whom correspondence should be addressed: bsaha@jncasr.ac.in and bivas.mat@gmail.com

ABSTRACT

Since the initial development of semiconductor heterostructures in the 1960s, researchers exploring the potential of artificially structured materials for applications in quantum electronic, optoelectronic, and energy conversion devices have sought a combination of metals and semiconductors, which could be integrated at the nanoscale with atomically sharp interfaces. Initial demonstration of such metal/semiconductor heterostructures employed elemental polycrystalline metal and amorphous semiconductors that demonstrated electronic tunneling devices, and more recently, such heterostructures were utilized to demonstrate several exotic optical phenomena. However, these metal/semiconductor multilayers are not amenable to atomic-scale control of interfaces, and defects limit their device efficiencies and hinder the possibilities of superlattice growth. Epitaxial single-crystalline TiN/Al_{0.72}Sc_{0.28}N metal/semiconductor superlattices have been developed recently and are actively researched for thermionic emission-based waste heat to electrical energy conversion, optical hyperbolic metamaterial, and hot-electron solar-to-electrical energy conversion devices. Most of these applications require controlled Schottky barrier heights that determine current flow along the cross-plane directions. In this Letter, the electronic band alignments and Schottky barrier heights in TiN/Al_{0.72}Sc_{0.28}N superlattice interfaces are determined by a combination of spectroscopic and first-principles density functional theory analyses. The experimental $E_F(\text{TiN}) - E_{VBM}(\text{Al}_{0.72}\text{Sc}_{0.28}\text{N})$ at the interfaces was measured to be 1.8 ± 0.2 eV, which is a bit smaller than that of the first-principles calculation of 2.5 eV. Based on the valence band offset and the bandgap of cubic-Al_{0.72}Sc_{0.28}N, an *n*-type Schottky barrier height of 1.7 ± 0.2 eV is measured for the TiN/Al_{0.72}Sc_{0.28}N interfaces. These results are important and useful for designing TiN/Al_{0.72}Sc_{0.28}N metal/semiconductor superlattice based thermionic and other energy conversion devices.

Published under license by AIP Publishing. <https://doi.org/10.1063/1.5126630>

Artificially structured materials such as epitaxial semiconductor superlattices (SLs) and heterostructures have been at the forefront of research, innovation, and development for over six decades to harness their novel and exotic physical properties for a range of fundamental physics studies, as well as electronic and optoelectronic device applications.^{1–6} Semiconductor SL metamaterials such as GaAs/AlAs have been utilized to demonstrate a range of

interesting physical properties such as quantum confinement of carriers, quantum well lasers, quantum cascade lasers, and resonant tunneling and are actively researched for the next generations of device technologies such as quantum computing, quantum information processing, subthreshold nanoelectronic switches.^{7–10} However, in comparison to the semiconductor SLs, the development of epitaxial lattice-matched metal/semiconductor SL

heterostructures has not progressed much primarily due to material compatibility and growth challenges.^{11–13}

Epitaxial single-crystalline TiN/Al_{0.72}Sc_{0.28}N metal/semiconductor SLs that exhibit lattice-matched interfaces and absence of extended defects have been developed recently.^{14–17} These nitride SLs crystallize in the rock salt structure and exhibit doping, alloying, and quantum size effects that are being actively utilized for engineering their physical properties.¹¹ Since metallic TiN possesses excellent plasmonic properties on par with traditional plasmonic materials such as Au,^{18–20} TiN/Al_{0.72}Sc_{0.28}N SLs have demonstrated hyperbolic dispersion of photonic isofrequency surfaces and large enhancements in the densities of photonic states that could be utilized for quantum electronic applications, subwavelength imaging, as well as for the demonstration of advanced theories of thermal conduction in materials such as hyper-thermal conductivity.^{14,15,21} Recent research on the semiconducting transition metal nitrides such as ScN and CrN and their solid solution alloys such as Sc_{1-x}Cr_xN and Sc_{1-x}Nb_xN has also demonstrated large thermoelectric power factors and potential for achieving a high thermoelectric “figure-of-merit” (ZT).^{22–24}

Fundamental to the thermionic emission-based waste heat to electrical energy conversion applications as well as for plasmon-induced hot-electron solar energy conversion devices such as, photocatalysts,²⁵ photodiodes,²⁶ and solar thermophotovoltaics,²⁷ it is necessary and important to control and engineer the Schottky barrier heights (ϕ_B) at metal/semiconductor interfaces since they eventually determine current flow across the cross-plane direction of the SLs.²⁸ Theoretical modeling has suggested that for high thermoelectric power factors through thermionic emission in metal/semiconductor SLs, a ϕ_B value of $\sim 10 K_B T$ would be ideal for filtering out the low energy electrons that would improve the Seebeck coefficient without reducing the electrical conductivity.^{29,30} Similarly, for plasmon-induced hot-electron transport across the metal/semiconductor interface, larger ϕ_B would be ideal. Nevertheless, the ability to control and tune ϕ_B from a few millielectron volts-to-several-electron-volts (from the terahertz-to-near-UV spectral range) in metal/semiconductor SLs would result in desired properties for many other types of device applications.

The determination the ϕ_B , however, is challenging. In the simplest picture of Schottky barrier formation that does not take into account the interfacial chemistry of barrier formation, the Mott-Schottky equation²⁸ predicts that $\phi_B = \psi - \chi$, where ψ and χ are the work function of the metal and electron affinity of the semiconductor, respectively. Interfacial lattice-mismatch, dangling bonds, charge transfer, and dipole and image charge formation, however, lead to Fermi level pinning in most elemental-metal/semiconductor interfaces, and the Mott-Schottky rule is not readily followed.^{31,32} Therefore, for any metal/semiconductor interfaces, ϕ_B needs to be carefully experimentally determined and properly modeled. The measurement of ϕ_B in metal/semiconductor interfaces is further complicated by fabrication induced leakage and the possibility of internal shunts that jeopardize the temperature-dependent electrical transport measurements, usually used for the ϕ_B estimation.^{33,34} For the TiN/Al_{0.72}Sc_{0.28}N SLs, the ϕ_B estimation has not been possible to date due to such device processing challenges, which have limited its practical applications in many ways. In this Letter, ϕ_B in TiN/Al_{0.72}Sc_{0.28}N metal/semiconductor SL interfaces is determined by X-ray photoelectron spectroscopy (XPS) and ultraviolet photoemission spectroscopy (UPS) analysis. Furthermore, first-principles DFT analysis is performed to understand the nature of band alignments and ϕ_B .

Four different films, (a) ~ 80 nm thick TiN, (b) ~ 120 nm thick Al_{0.72}Sc_{0.28}N deposited on 20 nm TiN, (c) 5 nm/5 nm, and (d) 3 nm/3 nm TiN/Al_{0.72}Sc_{0.28}N SLs having a total thickness of ~ 200 nm, were deposited by reactive dc-magnetron sputtering on (001) MgO substrates at a base pressure of $(2-4) \times 10^{-8}$ Torr at 750 °C (see the [supplementary material](#) for more details). X-ray diffraction revealed that all films grow with (002) orientations on (001) MgO substrates [see Fig. 1(a)]. Due to an approximate lattice-matching between TiN ($a = 4.24$ Å) and MgO ($a = 4.21$ Å), interference fringes arise in the XRD pattern of TiN that revealed its exact thickness. A 20 nm thick TiN seed layer was deposited on the MgO substrate before the Al_{0.72}Sc_{0.28}N film deposition, since the epitaxial stabilization technique was necessary for stabilizing the Al_{0.72}Sc_{0.28}N in the rock salt phase.^{11,14} Interference fringes from the bottom 20 nm TiN layer were also visible in the XRD pattern of Al_{0.72}Sc_{0.28}N/TiN/MgO, and the (002) peak was used to determine the c -axis lattice constant of 4.26 Å [see Fig. 1(a)]. The XRD pattern of the 5 nm/5 nm TiN/Al_{0.72}Sc_{0.28}N SL exhibits a (002) peak having a c -axis lattice constant of 4.25 Å and interference fringes arising due to the periodicity of the SL layers.

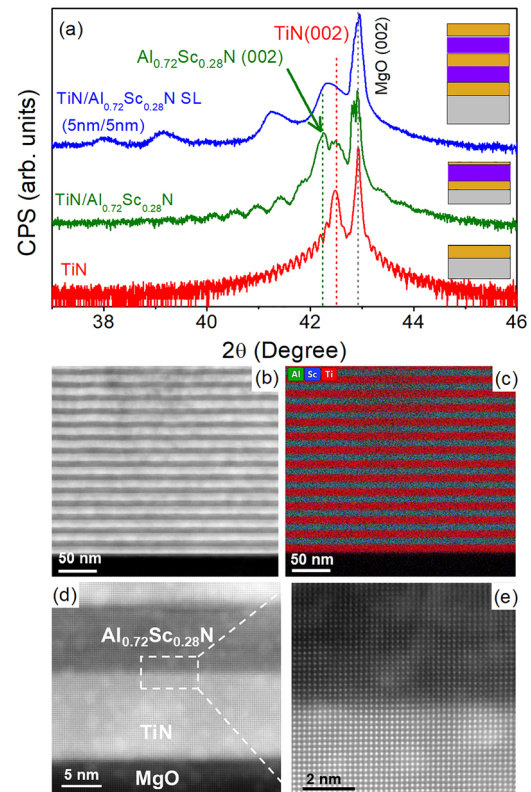


FIG. 1. (a) Symmetric 2θ - ω HR-XRD pattern of TiN, Al_{0.72}Sc_{0.28}N, and 5 nm/5 nm TiN/Al_{0.72}Sc_{0.28}N superlattices is presented, which shows (002) oriented crystal growth. (b) Layer-by-layer crystal growth with sharp interfaces is presented from high-angle annular dark-field-scanning-transmission-electron-microscopy (HAADF-STEM) analysis. (c) HRTEM-EDS elemental mapping of the layers exhibits sharp interfaces without any significant diffusion of atoms across layers. (d) TiN and Al_{0.72}Sc_{0.28}N lattice-fringes are presented with an inset in (e) showing the interface at higher magnification demonstrating cube-on-cube crystal growth without the presence of misfit-dislocations.

Representative high-resolution scanning transmission electron microscopy (HRSTEM) and energy-dispersive X-ray spectroscopy (EDS) elemental mapping of the SL layers further confirmed the structural properties [see Figs. 1(b) and 1(c)]. Lattice-matched and atomically sharp SL interfaces of metallic and semiconducting layers were visible in the HRSTEM images [see Fig. 1(d)], and cube-on-cube crystal growth having an epitaxial relationship of TiN [001] || Al_{0.72}Sc_{0.28}N [001] was established [see Fig. 1(e)].

Prior to the photoemission measurements, all films were cleaned with low energy (~1 keV) Ar⁺ ions to remove the surface contaminations, and an Au foil was used as a reference for Fermi energy standardization. The binding energies (BEs) of the core levels were determined using XPS [Al-K_α source (E_s = 1486.61 eV)], while the Fermi level of TiN [E_F(TiN)] and valence-band-maxima (VBM) of Al_{0.72}Sc_{0.28}N [E_{VBM}(Al_{0.72}Sc_{0.28}N)] were measured using UPS (He⁺ discharge lamp with E_s = 21.2182 eV). Both XPS and UPS binding energy measurements were recorded using the same spectrometer, and the samples were grounded to avoid any charging effects. Traditionally, the method proposed by Kraut *et al.*³⁵ is used for the determination of the valence band (VB) offsets between two semiconductors. We extend this procedure to determine the energy difference between the VBM of Al_{0.72}Sc_{0.28}N and the VB top (Fermi level) of TiN. The energy difference ΔE can be calculated from the following equation:

$$\begin{aligned} \Delta E = & [E_{\text{Ti-}2p_{3/2}}(\text{SL}) - E_{\text{Al-}2p}(\text{SL})] \\ & - [E_{\text{Ti-}2p_{3/2}}(\text{TiN}) - E_{\text{F}}(\text{TiN})] \\ & + [E_{\text{Al-}2p}(\text{Al}_{0.72}\text{Sc}_{0.28}\text{N}) - E_{\text{VBM}}(\text{Al}_{0.72}\text{Sc}_{0.28}\text{N})], \quad (1) \end{aligned}$$

where E_{Ti-2p_{3/2}}(SL) and E_{Al-2p}(SL) are the core level BE of the Ti-2p_{3/2} and Al-2p orbitals in the SL, respectively, while E_{Ti-2p_{3/2}}(TiN) and E_{Al-2p}(Al_{0.72}Sc_{0.28}N) are the core level BE of the TiN and Al_{0.72}Sc_{0.28}N thin film, respectively, in their isolated form. With the knowledge of ΔE for the metal-semiconductor interface and the bandgap of the semiconductor, the *n*-type φ_B is determined by the expression, φ_B = E_g^{Expt} - ΔE.

The BE of the core levels was determined by deconvolution of the photoemission spectra with a Voigt function (Gaussian: Lorentzian = 80%:20%) (see Fig. 2). Due to spin-orbit coupling, the Ti-2p orbitals split into two states, 2p_{3/2} and 2p_{1/2}, respectively. Along with the main Ti-2p peak corresponding to the Ti-2p-N bonds located at 455.65 ± 0.1 eV, Fig. 2 also shows the presence of two additional peaks. The BE peak at 459.01 ± 0.1 eV corresponds to Ti-O_x bonds that were also observed previously in the literature.³⁶ However, the peak centered at 457.0 ± 0.1 eV results from a multiple of factors such as shake-up and the presence of oxy-nitride (Ti-O-N) and could have contributions from plasmons, inelastically scattered electrons, multiple splitting, etc. as also reported previously.³⁷⁻⁴¹ The BE of Ti-2p_{3/2} and Ti-2p_{1/2} states for Ti 2p-N bonds from the TiN thin film and from the TiN/Al_{0.72}Sc_{0.28}N SL (see Fig. 2) exhibits a similar extent of spin-orbit splitting (5.8 ± 0.14 eV). While the FWHM of different Ti-2p states in TiN as well as in TiN/Al_{0.72}Sc_{0.28}N SL is similar to one another (see Fig. 2), it is important to note that the Ti-O_x-N_y and Ti-O_x peaks are much broader compared to the Ti-N, suggesting nonstoichiometric incorporation of oxygen in films. The presence of a minor amount of oxygen is not surprising as some amount of oxygen

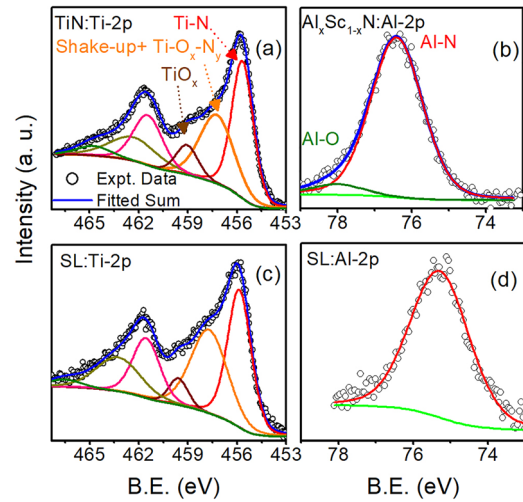


FIG. 2. XPS core level spectra of (a) Ti-2p and (b) Al 2p orbitals in TiN and Al_{0.72}Sc_{0.28}N thin films are presented, respectively. Along with the main Ti-2p-N bond peaks in (a), two other peaks are observed. XPS core level spectra of (c) Ti-2p and (d) Al-2p orbitals from TiN/Al_{0.72}Sc_{0.28}N SL are presented.

could still remain on the sample surface, even though the surface of the films was cleaned before the photoemission measurements. At the same time, though the thin films were deposited in high vacuum, background H₂O, CO₂, etc. could lead to a small amount of oxygen incorporation in the films, which was also previously found in ScN.⁴² The presence of such a small amount of oxygen, however, should not affect the band offset and φ_B measurements as discussed in the [supplementary material](#). The BE of Al 2p-N and Al 2p-O bonds in Al_{0.72}Sc_{0.28}N thin films was found to be centered at 76.4 ± 0.1 eV and 78.0 ± 0.1 eV, respectively, with a very similar FWHM of 1.65 eV. The BE of the Al-2p orbital of Al_{0.72}Sc_{0.28}N inside the SL was found to be centered at 75.3 ± 0.1 eV (Table I).

For the ΔE determination, along with the knowledge of the core-level peak positions, the VBM of Al_{0.72}Sc_{0.28}N and Fermi level of TiN are also required [see Eq. (1)]. UPS measurements were used to determine the VB positions with respect to the Fermi level. A clear metallic character is observed for the TiN thin film [see Fig. 3(a)], and the Fermi level (E_F) was located at 0 eV. The VB spectrum of Al_{0.72}Sc_{0.28}N showed semiconducting behavior, and a linear extrapolation of the leading edge to the baseline yields E_{VBM}-E_F to be -3.0 ± 0.1 eV

TABLE I. The binding energies (BEs) of Ti-2p_{3/2} for Ti 2p-N, Ti 2p-O_x-N_y, and Ti 2p-O_x bonds and Al-2p from the thin films and from the TiN/Al_{0.72}Sc_{0.28}N SL are presented.

Chemical bonding	BE in the SL configuration (eV)	BE in isolated films (eV)
Ti2p _{3/2} -N	455.8 ± 0.1	455.7 ± 0.1
Shake up + Ti2p _{3/2} -O _x -N _y	457.7 ± 0.1	457.2 ± 0.1
Ti2p _{3/2} -O _x	459.6 ± 0.1	459.1 ± 0.1
Al2p-N	75.3 ± 0.1	76.4 ± 0.1
Al2p-O	...	78.0 ± 0.1

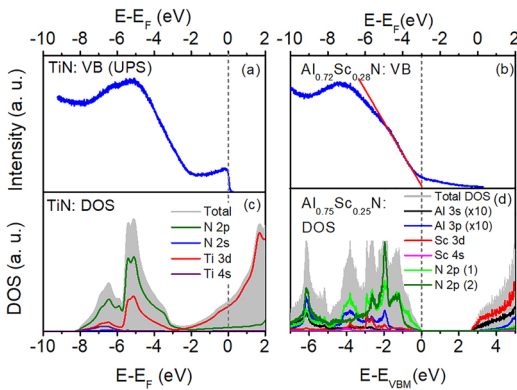


FIG. 3. UPS valence band spectra of (a) TiN and (b) $\text{Al}_{0.72}\text{Sc}_{0.28}\text{N}$ thin films are presented. The metallic character of TiN is represented by the sharp decrease in DOS at the Fermi level, while an $E_{\text{VBM}}-E_{\text{F}}$ value of -3.0 eV is measured for $\text{Al}_{0.72}\text{Sc}_{0.28}\text{N}$ from the UPS spectrum. The total and partial electronic DOS of (c) TiN and (d) $\text{Al}_{0.72}\text{Sc}_{0.28}\text{N}$ in their bulk configurations are presented that matched well with UPS measurements.

[Fig. 3(b)]. As previous optical measurements⁴³ have suggested the bandgap of $\text{Al}_{0.72}\text{Sc}_{0.28}\text{N}$ to be 3.5 eV , it suggests that as-grown $\text{Al}_{0.72}\text{Sc}_{0.28}\text{N}$ is an n -type degenerate semiconductor with Fermi energy on film surfaces that are close to the conduction band. The n -type carrier density of $(5-6) \times 10^{19}\text{ cm}^{-3}$ was measured previously⁴³ for the rock salt- $\text{Al}_{0.72}\text{Sc}_{0.28}\text{N}$, which would explain its n -type degenerate semiconducting nature.

Using the core-level BE, the Fermi level of TiN [$E_{\text{F}}(\text{TiN})$], and the VBM of $\text{Al}_{0.72}\text{Sc}_{0.28}\text{N}$ [$E_{\text{VBM}}(\text{Al}_{0.72}\text{Sc}_{0.28}\text{N})$], the ΔE value in the TiN/ $\text{Al}_{0.72}\text{Sc}_{0.28}\text{N}$ metal/semiconductor SL interface is measured to be $1.8 \pm 0.2\text{ eV}$ [see the band alignments in Fig. 4(a)]. The Schottky barrier height (ϕ_{B}) is also calculated using the simple relation, $\phi_{\text{B}} = E_{\text{g}}^{\text{Expt}}(\text{Al}_{0.72}\text{Sc}_{0.28}\text{N}) - \Delta E$, to be $1.7 \pm 0.2\text{ eV}$.

ΔE is further validated with the DFT calculations using plane wave basis with generalized gradient approximation (GGA) (see Sec. A of the supplementary material for details). Calculations suggest that TiN and $\text{Al}_{0.75}\text{Sc}_{0.25}\text{N}$ exhibit lattice constants of 4.24 \AA and 4.23 \AA , respectively, both of which are close to the experimental reports^{14,43} $a_{\text{TiN}} = 4.24\text{ \AA}$ and $a_{\text{Al}_{0.75}\text{Sc}_{0.25}\text{N}} = 4.26\text{ \AA}$. Electronic structure calculations of $\text{Al}_{0.75}\text{Sc}_{0.25}\text{N}$ showed a bandgap of 2.67 eV , which is significantly smaller than the experimentally measured bandgap of 3.5 eV in spite of the use of an onsite Coulomb interaction energy ($U = 3.5\text{ eV}$) in Sc $3d$ states within DFT+ U formalism, which otherwise captures the correct bandgap of ScN.⁴⁴ Atom projected DOS and its comparison with UPS measurements [Figs. 3(a) and 3(c)] revealed that VB of TiN is majorly composed of Ti- $3d$ and N- $2p$ orbitals, whereas the conduction band (CB) has predominantly Ti- $3d$ character. UPS spectra also showed that TiN exhibits metallic characteristics, with Ti- $3d$ orbitals dominating states close to the Fermi energy. While VB of $\text{Al}_{0.75}\text{Sc}_{0.25}\text{N}$ is primarily composed of N- $2p$ and Sc- $3d$ orbitals with a little contribution from Al- $3p$ states, the CB has a dominant character of Sc- $3d$ and Al- $3s$ orbitals [see Figs. 3(b) and 3(d)]. The underestimation of the bandgap, despite the use of a relatively larger value of U , is due to the fact that Al $3s$ states contribute significantly to the CB edges, which is unaffected by the inclusion of U [see Fig. 3(d)]. Without the Hubbard U correction, the bandgap was even smaller at 2.10 eV . Such underestimation of the bandgap of semiconductors is well-known for DFT

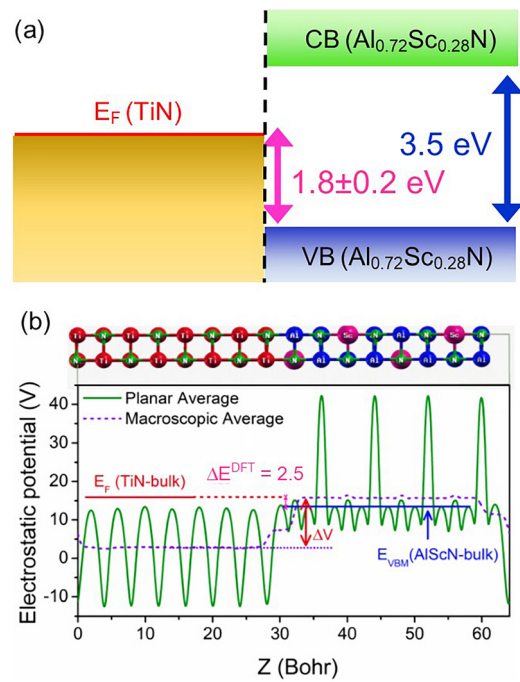


FIG. 4. (a) Experimental determination of the band alignment and $E_{\text{F}}(\text{TiN})-E_{\text{VBM}}(\text{Al}_{0.72}\text{Sc}_{0.28}\text{N})$ in the TiN/ $\text{Al}_{0.72}\text{Sc}_{0.28}\text{N}$ SL interface is presented. (b) Planar and macroscopic average electrostatic potential of the TiN/ $\text{Al}_{0.72}\text{Sc}_{0.28}\text{N}$ SL interface along the z -axis is presented. E_{F} (TiN-bulk) and E_{VBM} (AlScN-bulk) are calculated with respect to the average of the electrostatic potential in each of these material's bulk configurations. A schematic view of the TiN/ $\text{Al}_{0.75}\text{Sc}_{0.25}\text{N}$ interface is shown in the top.

calculations.⁴⁵ However, this underestimation should not significantly affect the VB offset calculations, as it is the excited states (CB) that are not properly captured in DFT calculations usually.

ΔE^{DFT} is obtained with the macroscopic averaging of the electrostatic potential alignment technique⁴⁶⁻⁴⁹ and expressed in the following equation:

$$\Delta E^{\text{DFT}} = E_{\text{F}}^{\text{DET}}(\text{TiN}) - E_{\text{VBM}}^{\text{DFT}}(\text{Al}_{0.75}\text{Sc}_{0.25}\text{N}) - \Delta V^{\text{DFT}}, \quad (2)$$

where ΔV^{DFT} is the change in the average electrostatic potential across the interface (positive if higher on the semiconductor side). To neutralize size effects, TiN/ $\text{Al}_{0.75}\text{Sc}_{0.25}\text{N}$ supercells with a thickness of $\sim 34\text{ \AA}$ [17 \AA (TiN)/ 17 \AA ($\text{Al}_{0.75}\text{Sc}_{0.25}\text{N}$)], corresponding to a 4-unit cell thickness of TiN and $\text{Al}_{0.75}\text{Sc}_{0.25}\text{N}$ each, along the cross-plane direction were constructed [see the top panel of Fig. 4(b)]. The microscopic averaging of the electrostatic potential in the TiN and $\text{Al}_{0.75}\text{Sc}_{0.25}\text{N}$ layers was smooth [see Fig. 4(b)]. The planar average of the electrostatic potential for $\text{Al}_{0.75}\text{Sc}_{0.25}\text{N}$ showed variations in peak heights due to the difference in atomic characteristics in crystal planes. Nevertheless, a clear and well-pronounced difference in the average electrostatic potential across the interface is obtained ($\Delta V = 12.8\text{ eV}$), and along with separately calculated $E_{\text{F}}^{\text{DET}}(\text{TiN})$ and $E_{\text{VBM}}^{\text{DFT}}(\text{Al}_{0.75}\text{Sc}_{0.25}\text{N})$ [also shown in Fig. 4(b)], the TiN/ $\text{Al}_{0.75}\text{Sc}_{0.25}\text{N}$ interface ΔE^{DFT} of 2.50 eV is calculated. Since the experimentally determined VB offset was $1.8 \pm 0.2\text{ eV}$, the DFT calculation result seems to be a bit higher. Several factors such as a difference in the amount of charge transfer, effects of a small

amount of interface and trap states, interfacial mixing at the atomic scale, and the formation of oxygen-related defects, clusters, nitrogen vacancies, etc. could have contributed to this overestimation by modeling.^{46,50} Nevertheless, the theoretical calculations provide a nuanced understanding and qualitative description of band alignment in SLs.

The measured ϕ_B value of 1.7 ± 0.2 eV in the TiN/Al_{0.72}Sc_{0.28}N metal/semiconductor interface seems to be ideal for SL based devices to achieve high-efficiency solar-energy conversion devices such as photocatalysts, photodiodes, and solar thermophotovoltaics through the thermionic transport of hot electrons across the metal/semiconductor interfaces. However, for thermoelectric applications, the measured Schottky barrier height seems to be a bit large compared to the calculations from the theoretical analysis. Therefore, further work related to the optimization of the barrier height would be necessary for achieving desired device properties.

In conclusion, the band alignments and Schottky barrier height in epitaxial single-crystalline TiN/Al_{0.72}Sc_{0.28}N metal/semiconductor SL interfaces are determined using photoemission spectroscopy and validated by first-principles DFT calculations. The experimental measurement suggests a Schottky barrier height of 1.7 ± 0.2 eV. Theoretical analysis with macroscopic averaging of the electrostatic potential technique overestimates the experimental valence band offset. The determination of the valence band offset and the Schottky barrier height of TiN/Al_{0.72}Sc_{0.28}N metal/semiconductor SL is a significant step in designing SL based thermionic emission devices such as hot-electron plasmonic nanostructures for solar energy conversion and thermoelectric energy conversion for waste-heat to electrical conversion applications.

See the [supplementary material](#) for information related to the growth of thin films and superlattices, details about the numerical simulation technique, Schottky barrier results for the 3 nm/3 nm superlattice, and details about the chemical integrity of the samples as well as band bending analysis at the metal/semiconductor interface.

B.S. and S.N. acknowledge the International Center for Materials Science (ICMS) and Sheikh Saqr Laboratory (SSL) in JNCASR for financial support and Center for Computational Materials Science (CCMS) for assistance. S.A. acknowledges DST-SERB for financial support. T.G. and M.B. thank Suvankar Paul for his help during PES measurements. M.G. acknowledges the facilities of the Microscopy Australia node at the University of Sydney (Sydney Microscopy and Microanalysis).

REFERENCES

- W. R. Frensley, in *Heterostructures Quantum Devices*, edited by N. G. Einspruch and W. R. Frensley (Elsevier, 1994), pp. 1–24.
- D. C. Tsui, H. L. Stormer, and A. C. Gossard, *Phys. Rev. Lett.* **48**, 1559 (1982).
- R. B. Laughlin, *Phys. Rev. Lett.* **50**, 1395 (1983).
- J. Faist, F. Capasso, D. L. Sivco, C. Sirtori, A. L. Hutchinson, and A. Y. Cho, *Science* **264**, 553 (1994).
- L. Esaki, *IEEE J. Quantum Electron.* **22**, 1611 (1986).
- S. Nakamura, M. Senoh, S. Nagahama, N. Iwasa, T. Yamada, T. Matsushita, H. Kiyoku, and Y. Sugimoto, *Jpn. J. Appl. Phys., Part 2* **35**, L74 (1996).
- K. Fujiwara, A. Nakamura, Y. Tokuda, T. Nakayama, and M. Hirai, *Appl. Phys. Lett.* **49**, 1193 (1986).
- Y. Horikoshi, M. Kawashima, and H. Yamaguchi, *Jpn. J. Appl. Phys., Part 2* **25**, L868 (1986).
- C. Sirtori, H. Page, C. Becker, and V. Ortiz, *IEEE J. Quantum Electron.* **38**, 547 (2002).
- E. E. Mendez, W. I. Wang, B. Ricco, and L. Esaki, *Appl. Phys. Lett.* **47**, 415 (1985).
- B. Saha, A. Shakouri, and T. D. Sands, *Appl. Phys. Rev.* **5**, 021101 (2018).
- T. Sands, C. J. Palmstrom, J. P. Harbison, V. G. Keramidas, N. Tabatabaie, T. L. Cheeks, R. Ramesh, and Y. Silberberg, *Mater. Sci. Rep.* **5**, 99 (1990).
- J. G. Zhu, C. B. Carter, C. J. Palmstrom, and S. Mounier, *Appl. Phys. Lett.* **56**, 1323 (1990).
- B. Saha, G. V. Naik, S. Saber, C. Akatay, E. A. Stach, V. M. Shalaev, A. Boltasseva, and T. D. Sands, *Phys. Rev. B* **90**, 125420 (2014).
- G. V. Naik, B. Saha, J. Liu, S. M. Saber, E. A. Stach, J. M. K. Irudayaraj, T. D. Sands, V. M. Shalaev, and A. Boltasseva, *Proc. Natl. Acad. Sci.* **111**, 7546 (2014).
- B. Saha, Y. R. Koh, J. Comparan, S. Sadasivam, J. L. Schroeder, M. Garbrecht, A. Mohammed, J. Birch, T. Fisher, A. Shakouri, and T. D. Sands, *Phys. Rev. B* **93**, 045311 (2016).
- M. Garbrecht, J. L. Schroeder, L. Hultman, J. Birch, B. Saha, and T. D. Sands, *J. Mater. Sci.* **51**, 8250 (2016).
- G. V. Naik, J. L. Schroeder, X. Ni, A. V. Kildishev, T. D. Sands, and A. Boltasseva, *Opt. Mater. Express* **2**, 478 (2012).
- U. Guler, A. Boltasseva, and V. M. Shalaev, *Science* **344**, 263 LP (2014).
- A. Lalis, G. Tessier, J. Plain, and G. Baffou, *Sci. Rep.* **6**, 38647 (2016).
- M. Garbrecht, L. Hultman, M. H. Fawey, T. D. Sands, and B. Saha, *J. Mater. Sci.* **53**, 4001 (2018).
- P. Eklund, S. Kerdsonpanya, and B. Alling, *J. Mater. Chem. C* **4**, 3905 (2016).
- M. A. Moram and S. Zhannig, *J. Mater. Chem.* **2**, 6042 (2014).
- B. Biswas and B. Saha, *Phys. Rev. Mater.* **3**, 20301 (2019).
- C. Clavero, *Nat. Photonics* **8**, 95 (2014).
- H. Chalabi, D. Schoen, and M. L. Brongersma, *Nano Lett.* **14**, 1374 (2014).
- A. Datas, *Appl. Phys. Lett.* **108**, 143503 (2016).
- J. Robertson, *J. Vac. Sci. Technol., B* **18**, 1785 (2000).
- D. Vashaee and A. Shakouri, *J. Appl. Phys.* **95**, 1233 (2004).
- D. Vashaee and A. Shakouri, *Phys. Rev. Lett.* **92**, 106103 (2004).
- R. T. Tung, *Appl. Phys. Rev.* **1**, 11304 (2014).
- T. J. Drummond, *Phys. Rev. B* **59**, 8182 (1999).
- J. Werner, A. F. J. Levi, R. T. Tung, M. Anzlowar, and M. Pinto, *Phys. Rev. Lett.* **60**, 53 (1988).
- B. Bati, Ç. Nuhoğlu, M. Sağıglam, E. Ayyıldız, and A. Türüt, *Phys. Scr.* **61**, 209 (2000).
- E. A. Kraut, R. W. Grant, J. R. Waldrop, and S. P. Kowalczyk, *Phys. Rev. Lett.* **44**, 1620 (1980).
- M.-H. Chan and F.-H. Lu, *Thin Solid Films* **517**, 5006 (2009).
- I. Bertoti, M. Mohai, J. L. Sullivan, and S. O. Saied, *Appl. Surf. Sci.* **84**, 357 (1995).
- D. Jaeger and J. Patscheider, *J. Electron Spectrosc. Relat. Phenom.* **185**, 523 (2012).
- B. J. Burrow, A. E. Morgan, and R. C. Ellwanger, *J. Vac. Sci. Technol., A* **4**, 2463 (1986).
- L. Porte, L. Roux, and J. Hanus, *Phys. Rev. B* **28**, 3214 (1983).
- N. C. Saha and H. G. Tompkins, *J. Appl. Phys.* **72**, 3072 (1992).
- B. Saha, M. Garbrecht, J. A. Perez-Taborda, M. H. Fawey, Y. R. Koh, A. Shakouri, M. Martin-Gonzalez, L. Hultman, and T. D. Sands, *Appl. Phys. Lett.* **110**, 252104 (2017).
- B. Saha, S. Saber, G. V. Naik, A. Boltasseva, E. A. Stach, E. P. Kvam, and T. D. Sands, *Phys. Status Solidi* **252**, 251 (2015).
- B. Saha, J. Acharya, T. D. Sands, and U. V. Waghmare, *J. Appl. Phys.* **107**, 33715 (2010).
- J. Heyd, J. E. Peralta, G. E. Scuseria, and R. L. Martin, *J. Chem. Phys.* **123**, 174101 (2005).
- N. R. D'Amico, G. Cantele, and D. Ninno, *Appl. Phys. Lett.* **101**, 141606 (2012).
- J. Junquera, M. H. Cohen, and K. M. Rabe, *J. Phys.: Condens. Matter* **19**, 213203 (2007).
- L. Colombo, R. Resta, and S. Baroni, *Phys. Rev. B* **44**, 5572 (1991).
- A. Baldereschi, S. Baroni, and R. Resta, *Phys. Rev. Lett.* **61**, 734 (1988).
- K. Xiong, W. Wang, D. M. Zhernokletov, K. C. Santosh, R. C. Longo, R. M. Wallace, and K. Cho, *Appl. Phys. Lett.* **102**, 22901 (2013).